European Journal of Mechanics B/Fluids 28 (2009) 420–429

Contents lists available at ScienceDirect

European Journal of Mechanics B/Fluids

www.elsevier.com/locate/ejmflu

Non-linear wave interactions from transient growth in plane-parallel shear flows

L. Håkan Gustavsson *

Division of Fluid Mechanics, Luleå University of Technology, S-97187 Luleå, Sweden

ARTICLE INFO

Article history:
Received 27 March 2008
Received in revised form 7 October 2008
Accepted 9 October 2008
Available online 15 October 2008

Keywords:
Parallel shear flows
Transient growth
Non-linear wave interaction

ABSTRACT

Based on the normal velocity–normal vorticity (v–η) formulation for the development of 3D disturbances in plane-parallel shear flows, the non-linear terms in the governing equations are derived as convolution integrals of the Fourier-transformed variables. They are grouped in three categories: v–v, v–η and η–η terms, and are expressed in a simple geometric form using the modulus of the two wave-vectors ($\mathbf{k}'$ and $\mathbf{k}''$) appearing in the convolution integrals, and their intervening angle (χ). The non-linear terms in the v-equation involving η are all weighted by $\sin\chi$ (or $\sin^2\chi$). This confirms the known result that non-linear regeneration of normal velocity, necessary for a sustained driving of 3D disturbances, is not possible for stream-wise elongated structures ($\alpha = 0$), only. It is therefore suggested how transiently amplified η can interact with *decaying* 2D waves to activate (oblique) waves which may be less damped than the 2D wave. This is shown to be possible for Blasius flow. In the η-equation, non-linear effects *are* possible for elongated structures resulting in shorter spanwise scales appearing at a shorter time-scale than the (linear) transient growth. A numerical example shows the details of this process in plane Poiseuille flow. From an inspection of the y-dependency (wall-normal direction) of the non-linear terms it is suggested that higher y-derivatives may give rise to non-linear effects in the inviscid development of perturbations. Also, a result for the y-symmetry of the non-linear terms is derived, applicable to plane Poiseuille flow.

1. Introduction

Many recent studies of the stability of plane-parallel (and some other) shear flows have been concerned with the mechanism of transient growth. Essentially vortex stretching and tilting, this mechanism produces largest energy response from initial disturbances consisting of longitudinal vortices (see e.g. Butler and Farrell [1], for an early reference) the response being streaks elongated in the stream-wise direction. Thus, a motion in the cross-stream plane is transformed to a motion in the horizontal plane with the normal velocity perturbation decaying. The mechanism operates at sub-critical Reynolds numbers and the energy growth is considerable, in fact so large that it is only exponential growth on inflexion profiles that can compete (see e.g. Corbett and Bottaro [2]). Therefore, it is a prime candidate mechanism to use in transition studies at sub-critical Reynolds numbers. It is also thought to be the mechanism for streak formation in near-wall turbulence and in fact, the numerical simulations of Kim and Lim [3] suggest that the linear forcing in transient growth is necessary for the maintenance of turbulence, with the proper scales supposedly set by non-linear processes.

The importance of transient growth in the laminar-to-turbulence transition process (and in turbulence) depends on how the normal velocity (v) can be regenerated. This does not occur for linearly developing infinitely elongated structures ($\alpha = 0$) since then the cross-stream velocity components (v and w), and thereby the streamwise vorticity, decouple from the streamwise velocity component and decay (Pearson and Abernathy [4]). In terms of the v–η (η = normal vorticity) formulation the decoupling shows up in the non-linear term in the v-equation which contains only decaying cross-stream components (Gustavsson [5]). Still, streaks have attracted considerable recent interest since several experimental investigations (see e.g. Matsubara and Alfredsson [6]), indicate that transition to turbulence in parallel shear flows is associated with unstable streaks. The basic idea is that streaks generate a spanwise modulation of the mean flow which changes the (exponential) stability properties of the flow. This model, originally developed for Görtler instability by Nayfeh [7] and formulated in the v–η frame for channel flows by Waleffe [8], assumes a *steady* spanwise modulation of the background flow, on which then (inviscid or viscous) *secondary* instabilities can operate. This model has been studied for boundary layers by e.g. Cossu and Brandt [9] and Andersson et al. [10], in channel flow by Waleffe [8] and Reddy et al. [11]. The appearing instability is generally considered inflexional but requires large streak amplitudes to operate (see e.g. Andersson et al. [10]). Also, it has recently (Cossu and Brandt [12]) been shown that streaks can, depending on the streak amplitude, both desta-

* Tel.: +46(0)920491283; fax: +46(0)920491074.
E-mail address: hakan.gustavsson@ltu.se.

0997-7546/$ – see front matter
doi:10.1016/j.euromechflu.2008.10.001

bilize and dampen 2D Tollmien–Schlichting (TS) waves. The latter possibility has been used in an interesting experimental study by Fransson et al. [13], where TS wave growth is hindered by suitably designed streaks generated by cylinder elements. The ambiguous results that streaks may both destabilize and stabilize TS waves suggest that further detailed work is required to clarify their role in the transition process.

Streaks appear also in transition models and in Schmid and Henningson [14], Chapter 9, an account is given for the various scenarios, all based on streak instabilities. The transition model that does not assume streaks at the outset is the oblique transition model of Schmid and Henningson [15]. In this model, a pair of oblique waves $(1, \pm 1)$ is made to interact non-linearly to generate, among other structures, a spanwise periodic perturbation $(0, 2)$ which is then subject to transient growth. This is followed by a streak instability provided the amplitude becomes sufficiently large. Therefore, it relies on the same secondary instability as other streak-based models. However, the oblique transition has a feature which may be the key to its relative success and which will be elaborated on in the discussion of the present paper.

Even in fully developed near-wall turbulence, streak instabilities form an important part of the regeneration cycle as demonstrated by Hamilton et al. [16], the details of which seem quite complicated, however. As turbulence is not the subject of the present paper, we refer to this article for details, and to the subsequent work of Jimenez and Pinelli [17] and Schoppa and Hussain [18].

The above studies show the importance of streaks in the transition process but rely on already established streaks as a mean flow modification for secondary instabilities. Thus, they do not address the *intrinsic* non-linear properties of transient growth as seen from an initial value approach. That is, how does the strong (linear) transient growth develop non-linearities from the available initial perturbations? This is conceptually different from the streak stability studies where certain perturbations are allowed to develop on a viscous time scale (to form streaks) whereas others are allowed to develop inviscidly *after* the streaks have been established. This *secondary* approach calls for a consistent time-scaling procedure to distinguish between the different types of perturbations. (In Chapman [19], an asymptotics-based time-scale analysis of transient growth has been developed.)

It is the main purpose of the present paper to investigate the *primary* non-linear interactions of transient growth as revealed by the non-linear terms in the governing equations in the v–η formulation, seen from an initial-value perspective. Thus, it is assumed that a (small) initial perturbation first develops according to the linearized equations, and knowing that certain terms (involving η) grow in time, non-linear terms will eventually become important. A full analysis of this process needs a Reynolds number scaling of the amplitudes (cf. Chapman [19]) but this aspect is not considered in the present work.

The analytical approach used is a continuous wave-interaction formulation, since transient growth operates in a fairly broad wave number range, and involves the use of Fourier transform techniques where non-linearities appear as convolution integrals. In the analysis section, the necessary mathematical background is given, with the details explained in Appendix A. A new geometrical interpretation of the convolution integrands is here introduced by which the non-linear terms are first qualitatively assessed. Motivated by the theoretical observations, a numerical study is then made of the non-linear self-modulation of the normal vorticity for streamwise elongated ($\alpha = 0$) structures in plane Poiseuille flow. For this case, analytical solutions of the linear problem are used.

Since the v–η formulation breaks down when both the streamwise and the spanwise wave numbers equal zero ($\alpha = \beta = 0$), a separate study is made for this case, presented in Appendix B. Intended to simplify the evaluation of the convolution integrals, it is also shown in Appendix C how the values of the Fourier transforms of v and η can be related to values in the first quadrant of the Fourier plane.

Whereas the main focus of the paper is to show the possible non-linear wave-interactions in the Fourier plane, the analytical results also allow some conclusions to be drawn about properties in the wall-normal direction (y) of the non-linear terms.

The paper is concluded with a discussion of how the geometrical model can be used to show how *decaying* Orr–Sommerfeld (O–S) modes can interact with transiently growing η to produce oblique waves with less damping than the ingredient O–S mode, applicable to Blasius flow. Here, a theoretical motivation for the oblique transition model of Schmid and Henningson [15] is also given.

2. Analysis

The governing equations for the development of perturbations in plane-parallel shear flows are conveniently written in the normal velocity/normal vorticity (v–η) formulation (see e.g. Schmid and Henningson [14], p. 156)

$$\left(\frac{\partial}{\partial t} + U\frac{\partial}{\partial x}\right)\nabla^2 v - U''\frac{\partial v}{\partial x} + N_v = \frac{1}{R}\nabla^4 v \tag{1}$$

and

$$\left(\frac{\partial}{\partial t} + U\frac{\partial}{\partial x}\right)\eta + U'\frac{\partial v}{\partial z} + N_\eta = \frac{1}{R}\nabla^2 \eta \tag{2}$$

where the standard coordinate notation for this type of flows is used i.e. with x in the mean flow direction, y in the shear direction and z in the cross flow direction. R is the Reynolds number and $U = U(y)$ is the mean flow, with primes denoting y-derivatives. The non-linear terms are given by

$$N_v = \left(\frac{\partial^2}{\partial x^2} + \frac{\partial^2}{\partial z^2}\right)S_2 - \frac{\partial}{\partial y}\left(\frac{\partial S_1}{\partial x} + \frac{\partial S_3}{\partial z}\right) \tag{3}$$

and

$$N_\eta = \frac{\partial S_1}{\partial z} - \frac{\partial S_3}{\partial x} \tag{4}$$

where

$$S_i = \frac{\partial}{\partial x_j}(u_i u_j) \tag{5}$$

using index notation for simplicity. Finally, to obtain the other velocity components, continuity,

$$\frac{\partial u}{\partial x} + \frac{\partial w}{\partial z} = -\frac{\partial v}{\partial y} \tag{6}$$

and the definition of normal vorticity,

$$\frac{\partial u}{\partial z} - \frac{\partial w}{\partial x} = \eta \tag{7}$$

are used. Since the coordinates x and z are homogeneous in the flows of interest, Fourier transformations are applied in these coordinates, with transformation variables α and β, respectively. Eqs. (1) and (2) then become

$$\left(\frac{\partial}{\partial t} + \mathrm{i}\alpha U\right)(D^2 - k^2)\hat{v} - \mathrm{i}\alpha U''\hat{v} + \hat{N}_v = \frac{1}{R}(D^2 - k^2)^2\hat{v} \tag{8}$$

and

$$\left(\frac{\partial}{\partial t} + \mathrm{i}\alpha U\right)\hat{\eta} + \mathrm{i}\beta U'\hat{v} + \hat{N}_\eta = \frac{1}{R}(D^2 - k^2)\hat{\eta} \tag{9}$$

where, $D = d/dy$ and $k^2 = \alpha^2 + \beta^2$.

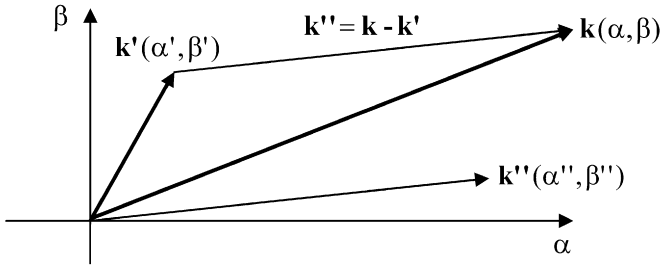

Fig. 1. Wave triad appearing in the convolution integrals.

Eqs. (6) and (7) give

$$\mathrm{i}\alpha\hat{u} + \mathrm{i}\beta\hat{w} = -D\hat{v} \tag{10a}$$

and

$$\mathrm{i}\beta\hat{u} - \mathrm{i}\alpha\hat{w} = \hat{\eta}. \tag{10b}$$

From (10), $\hat{u}$ and $\hat{w}$ are obtained in terms of $\hat{v}$ and $\hat{\eta}$ as

$$\hat{u} = \frac{\mathrm{i}\alpha}{k^2}D\hat{v} - \frac{\mathrm{i}\beta}{k^2}\hat{\eta} \tag{11}$$

and

$$\hat{w} = \frac{\mathrm{i}\beta}{k^2}D\hat{v} + \frac{\mathrm{i}\alpha}{k^2}\hat{\eta}. \tag{12}$$

Fourier transforming N_v and N_η gives

$$\begin{aligned}\hat{N}_v &= -k^2\hat{S}_2 - D\left(\mathrm{i}\alpha\hat{S}_1 + \mathrm{i}\beta\hat{S}_3\right)\\ &= -\left(D^2+k^2\right)(\mathrm{i}\alpha\widehat{u\upsilon} + \mathrm{i}\beta\widehat{\upsilon w})\\ &\quad + D\left(\alpha^2\hat{u}^2 + \beta^2\hat{w}^2 + 2\alpha\beta\widehat{uw} - k^2\hat{v}^2\right)\end{aligned} \tag{13}$$

and

$$\begin{aligned}\hat{N}_\eta &= \mathrm{i}\beta\hat{S}_1 - \mathrm{i}\alpha\hat{S}_3\\ &= \alpha\beta\left(\hat{w}^2 - \hat{u}^2\right) + \left(\alpha^2-\beta^2\right)\widehat{uw} + D(\mathrm{i}\beta\widehat{u\upsilon} - \mathrm{i}\alpha\widehat{\upsilon w}).\end{aligned} \tag{14}$$

But the Fourier transform of a product can be written as the convolution of the product of the transforms so, e.g.

$$\begin{aligned}\widehat{u\upsilon}(\alpha,\beta) &= \frac{1}{2\pi}\int_{-\infty}^{\infty}\int_{-\infty}^{\infty}\hat{u}(\alpha',\beta')\cdot\hat{v}(\alpha-\alpha',\beta-\beta')\,d\alpha'\,d\beta'\\ &\equiv \frac{1}{2\pi}\iint\hat{u}'\cdot\hat{v}''\,d\alpha'\,d\beta'\end{aligned} \tag{15}$$

where the simplified notation

$$\hat{u}' \equiv \hat{u}(\alpha',\beta') \quad\text{and}\quad \hat{v}'' \equiv \hat{v}(\alpha-\alpha',\beta-\beta') \tag{16}$$

is introduced. The wave vectors involved are $\mathbf{k} = (\alpha,\beta)$, $\mathbf{k}' = (\alpha',\beta')$ and $\mathbf{k}'' = (\alpha-\alpha',\beta-\beta')$ which thus form a standard wave triad ($\mathbf{k} = \mathbf{k}' + \mathbf{k}''$), illustrated in Fig. 1. When performing the convolution integrals, regions with large integrand amplitudes at both $\mathbf{k}'$ and $\mathbf{k}''$ should contribute most and adding the two vectors gives a $\mathbf{k}$-value with large non-linear response.

In the convolution integrands, $\hat{u}$ and $\hat{w}$ are now substituted for $\hat{v}$ and $\hat{\eta}$ according to (11) and (12), the details of which are given in Appendix A. There, a key step is to introduce the angle χ between $\mathbf{k}'$ and $\mathbf{k}''$ (counted positive going from $\mathbf{k}''$ to $\mathbf{k}'$). Sorting the different terms in $\hat{N}_v$ and $\hat{N}_\eta$ then yields (see also Davidsson [20]) the following integrands:

(a) $\hat{N}_v$

$$\begin{aligned}\hat{v}\text{–}\hat{v}\text{:}\ &\left(1+\frac{k''}{k'}\cos\chi\right)\left(D^2+k^2\right)(D\hat{v}'\cdot\hat{v}'')\\ &-\left(1+\frac{k''}{k'}\cos\chi\right)\left(1+\frac{k'}{k''}\cos\chi\right)D(D\hat{v}'\cdot D\hat{v}'')\\ &-k^2D(\hat{v}'\cdot\hat{v}'');\end{aligned} \tag{17}$$

$$\begin{aligned}\hat{v}\text{–}\hat{\eta}\text{:}\ &-\frac{k''}{k'}\sin\chi\left(D^2+k^2\right)(\hat{v}''\cdot\hat{\eta}') - \sin\chi\left(\frac{k'}{k''}+\cos\chi\right)D(D\hat{v}'\cdot\hat{\eta}'')\\ &+\sin\chi\left(\frac{k''}{k'}+\cos\chi\right)D(D\hat{v}''\cdot\hat{\eta}')\end{aligned} \tag{18}$$

$$\hat{\eta}\text{–}\hat{\eta}\text{:}\ \sin^2\chi\,D(\hat{\eta}'\cdot\hat{\eta}''). \tag{19}$$

(b) $\hat{N}_\eta$

$$\hat{v}\text{–}\hat{v}\text{:}\ \sin\chi\left(\frac{k''}{k'}D^2\hat{v}'\cdot\hat{v}'' - \cos\chi\,D\hat{v}'\cdot D\hat{v}''\right), \tag{20}$$

$$\begin{aligned}\hat{v}\text{–}\hat{\eta}\text{:}\ &-\sin^2\chi\,D\hat{v}'\cdot\hat{\eta}''\\ &+\left(\frac{k'}{k''}+\cos\chi\right)\left(\frac{k''}{k'}\hat{v}''\cdot D\hat{\eta}' - \cos\chi\,D\hat{v}''\cdot\hat{\eta}'\right);\end{aligned} \tag{21}$$

$$\hat{\eta}\text{–}\hat{\eta}\text{:}\ -\sin\chi\left(\frac{k'}{k''}+\cos\chi\right)\hat{\eta}'\cdot\hat{\eta}''. \tag{22}$$

The expressions (17)–(22) form the basis for assessing possible non-linear interactions in plane-parallel shear flows. By expanding the y-derivatives, further reductions are possible but the above form is convenient enough for the purposes of the present paper.

A general observation is that the expressions consist of combinations of: a constant, a trigonometric function of χ, k^2, and k'/k''. Of these, the trig functions never exceed unity whereas k^2 and k'/k'' may become large.

3. Interpretation of formulas (17)–(22)

The formulation with k', k'' and χ makes it possible to probe the (α,β) plane for potential non-linear interactions and an inspection of (17)–(22) will first be done to get an overall idea how non-linear effects may originate. The strategy is to use properties of the solution for the linear initial value problem and determine what non-linear terms are induced, primarily due to the linear growth of η, which is the dominant effect of transient growth. Whereas the first results are mainly qualitative, a numerical example is given in Section 4 how the formulas can be used for specific calculations. In the discussion, the generation of oblique waves is given some numerical background by considerations of the decay properties of the least damped O–S mode in Blasius flow.

The results are concerned mainly with the behaviour in the wave-number plane but a couple of interesting conclusions may be made by considering also the y-dependency of the non-linear terms.

3.1. Non-linearities in $\hat{N}_v$ due to growth of $\hat{\eta}$

The motivating interest for this study is the non-linear effects of the transient growth mechanism which gives large growth of the normal vorticity with optimum for streamwise elongated structures. Since the forcing v-perturbation decays in the subcritical Reynolds number regime, the mechanism's intrinsic ability for non-linear regeneration of $\hat{v}$ is of particular interest. Therefore, terms involving $\hat{\eta}$ in $\hat{N}_v$ are first considered. These terms, represented by (18) and (19), are all weighted by the factor $\sin\chi$ (or $\sin^2\chi$) which means that if $\mathbf{k}'$ and $\mathbf{k}''$ are aligned there is no contribution to the convolution integrals. Since large transient growth

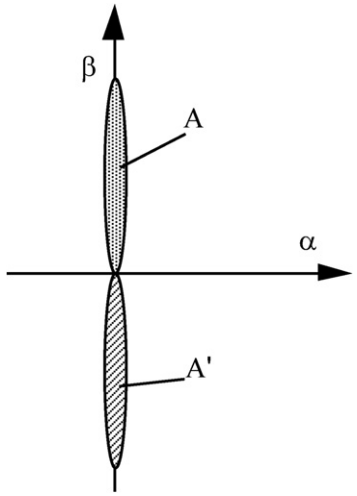

Fig. 2. Wave number areas with transient growth of η.

occurs for wave numbers in a narrow region around the β-axis, denoted A in Fig. 2, we can expect weak non-linear effects on $\hat{N}_v$ by growing $\hat{\eta}$, only. This result confirms the early observation that transiently growing infinitely elongated structures ($\alpha = 0$) are not able to non-linearly modify the normal velocity. Instead, largest non-linear contributions are to be expected from cases where $\mathbf{k}'$ and $\mathbf{k}''$ are orthogonal, but noting that $\sin(\pi/4) \sim 0.7$, contributions may also be significant from a wider range of χ. This is equivalent to Chapman's [19] conclusion that a strong coupling occurs between streamwise and oblique modes.

Since regeneration of $\hat{v}$ from only transiently growing $\hat{\eta}$ seems weak it is necessary to consider other mechanisms that produce growth in wave-number regions that can combine with region A to produce a strong non-linear response. The other possible linear growth mechanism is exponential which operates at higher Reynolds numbers than transient growth and applies to $\hat{v}$. Its area of growth is centered around the α-axis and widens towards the origin as the Reynolds number increases (region B in Fig. 3(c)). The resulting wave number from the non-linear interaction corresponds by necessity to an oblique wave as illustrated in Fig. 3(c). Unless the velocity profile is inflexional, the exponential growth is much weaker than transient growth (Corbett and Bottaro [2]) and at sub-critical Reynolds numbers the point P will always end up in a region with exponential decay of v-modes. However, the decay may not be too large at sub-critical Reynolds numbers and in the discussion we elaborate on this aspect in Blasius flow.

Finally, (19) suggests that also this term could contribute to $\hat{N}_v$ if $\mathbf{k}'$ and $\mathbf{k}''$ are orthogonal, as in Fig. 3(c). At $\mathbf{k}''$, $\beta = 0$ so transient growth of $\hat{\eta}''$ is not possible and the value of $\hat{\eta}''$ is essentially decided by its initial value. The temporal behaviour of $\hat{\eta}''$ is then given by the exponential decay rate of the vorticity modes which is always larger than that of the least damped Orr–Sommerfeld mode. In comparison with the $\hat{v}$–$\hat{\eta}$ interaction one can thus expect this term to be negligible but a full assessment of its importance will require more detailed (numerical) studies of the full wave number extent of transient growth.

3.2. Non-linearities in $\hat{N}_\eta$ due to growth of $\hat{\eta}$

For $\hat{N}_\eta$, (20)–(22) show that $\sin\chi$ does not appear in some of the $\hat{v}$–$\hat{\eta}$ terms (in (21)) which indicates that a non-linear modification of $\hat{\eta}$ *is* possible with $\mathbf{k}'$ and $\mathbf{k}''$ both in region A, giving a response at higher spanwise wave numbers, as indicated in Fig. 3(a). In the extreme case of excitation only on the β-axis, this non-linear process can be analyzed in more detail and a numerical example of its spanwise selectivity and temporal behaviour is given in the next section.

3.3. The case $\mathbf{k}' + \mathbf{k}'' = \mathbf{0}$

To fully assess the growth in region A, it is necessary to account also for the case that $\mathbf{k}'$ is in A and $\mathbf{k}''$ in the image region along the negative β-axis (A′ in Fig. 2). Then, the possibility of $\mathbf{k}' + \mathbf{k}'' = \mathbf{0}$ arises, shown in Fig. 3(b). In terms of k', k'' and χ this means that $k' = k''$ and $\chi = \pi$ and evaluation of (17)–(22) gives zero for all terms. At the point $\alpha = \beta = 0$, the v–η formulation thus breaks down and a separate analysis is required, conveniently based on the component equations. In Appendix B the details of this analysis are given and involve basically integration of the component equations in the x–z plane. For the v-component this quantity is always zero, it diffuses for the w-component and grows for the u component due to the growth of η.

3.4. y-derivatives

Another feature of (17)–(22) is the prevalence of y-derivatives. For inviscidly developing perturbations on an infinitely extended constant shear flow, it has been shown [20] that especially the highest derivatives, $D^3\hat{v}$ and $D^2\hat{\eta}$, may grow to considerable values. This is mainly due to the advective character of the inviscid development since differentiating an expression like $f(x-Ut)$ with respect to y produces algebraic t-terms. Davidsson's calculations

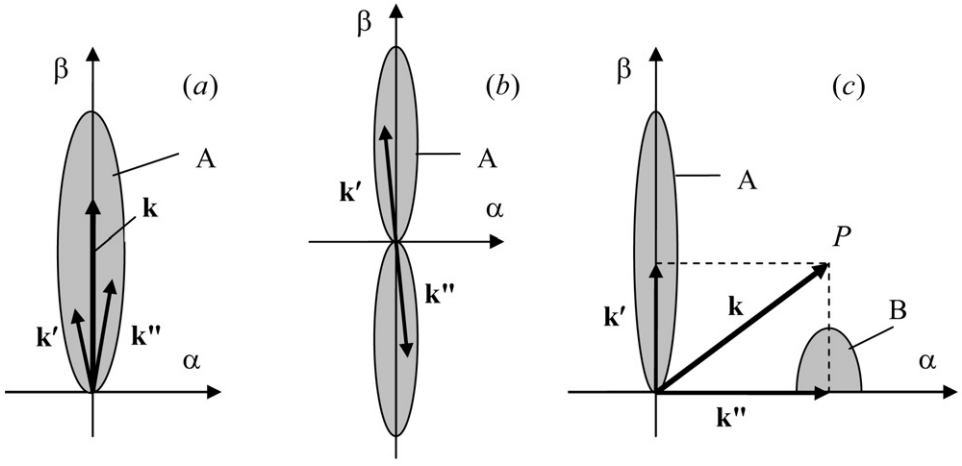

Fig. 3. Possible non-linear interactions due to transient growth of η: (a) v–η interaction in $\hat{N}_\eta$, (b) $\mathbf{k}' + \mathbf{k}'' = 0$ (mean flow correction), (c) v–η interaction in $\hat{N}_v$.

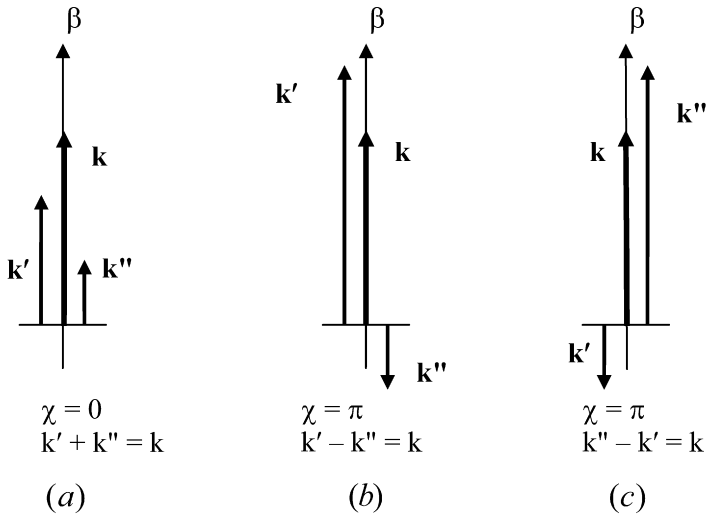

Fig. 4. Three possible configurations with $\mathbf{k}'$ and $\mathbf{k}''$ aligned on the β-axis such that $\mathbf{k}' + \mathbf{k}'' = \mathbf{k}$ is fixed.

also show that the main non-linear interaction in the inviscid case comes from the $\hat{\eta}$–$\hat{\eta}$ interaction which is consistent with the fact that $\hat{\eta}$ in that approximation does not decay but attains a constant value for large times ('the permanent scar').

A final deduction from the y-dependency comes from considering the y-symmetry of the non-linear terms, relevant for plane Poiseuille flow. In the linear problem, the forcing v-perturbation can be split into a symmetric and an anti-symmetric component where the symmetric part generates anti-symmetric η (and vice-versa). Noting that a y-derivative (D) changes the symmetry of the differentiated quantity, inspection of (17)–(22) shows that the terms in $\hat{N}_v$ are always anti-symmetric, independent of the original symmetries, whereas the terms in $\hat{N}_\eta$ are always symmetric. However, this applies only if the initial perturbation is *either* symmetric *or* anti-symmetric. For a mixed perturbation, interaction terms with the opposite symmetry will also be generated.

4. Numerical example: non-linear self-modulation of $\hat{\eta}$ for $\alpha = 0$

The results presented so far should give an idea how Eqs. (17)–(22) can be used as a theoretical framework for assessing non-linear interactions and a guideline for further analytical and numerical studies. A detailed evaluation of their potential implies numerical studies and we give an example in this section which will elaborate on the gained insights. It concerns the non-linear self modulation of $\hat{\eta}$ for infinitely elongated structures, with application to plane Poiseuille flow. In the discussion, a model is presented for the generation of oblique waves from the interaction of transiently growing η and decaying Orr–Sommerfeld modes with application to Blasius flow.

It was noticed in Section 3.2 that a non-linear feed-back due to growth of $\hat{\eta}$ for infinitely elongated structures ($\alpha = 0$) is possible only in $\hat{\eta}$ itself (Eq. (21)) and we will show how this process operates in a numerical example. The flow chosen is plane Poiseuille flow for which analytical solutions are available for $\alpha = 0$, [5]. The wave number geometry is basically that of Fig. 3(a), restricted to the extreme case of excitation on the β-axis only and with values defined also on the negative β-axis. With $\mathbf{k}'$ and $\mathbf{k}''$ aligned on the β-axis, and such that $\mathbf{k}$ ($= \mathbf{k}' + \mathbf{k}''$) is fixed, three different cases need to be considered, shown in Fig. 4. With values also on the negative β-axis, the two symmetry cases in z (cf. Appendix C for details) for the initial data (index $_0$) are considered:

(a) $v_0(-z) = v_0(z)$.

In the Fourier plane, this corresponds to the conditions $\hat{v}(-k') = \hat{v}(k')$ and $\hat{\eta}(-k') = -\hat{\eta}(k')$. Integration of the first remaining term in (21) along the β-axis $(-\infty, \infty)$ then gives (k' is used as integration variable)

$$I_a = \int_0^k \left(\frac{k'}{k''} + 1\right) \frac{k''}{k'} \hat{v}(k-k') D\hat{\eta}(k')\, dk'$$

$$= \int_0^k \frac{k}{k'} \hat{v}(k-k') D\hat{\eta}(k')\, dk', \tag{23a}$$

$$I_b = \int_k^\infty \left(\frac{k'}{k''} - 1\right) \frac{k''}{k'} \hat{v}(k-k') D\hat{\eta}(k')\, dk'$$

$$= \int_k^\infty \frac{k}{k'} \hat{v}(k'-k) D\hat{\eta}(k')\, dk', \tag{23b}$$

$$I_c = \int_0^\infty \left(\frac{k'}{k''} - 1\right) \frac{k''}{k'} \hat{v}(k+k') D\hat{\eta}(-k')\, dk'$$

$$= \int_0^\infty \frac{k}{k'} \hat{v}(k+k') D\hat{\eta}(k')\, dk' \tag{23c}$$

the sum of which becomes

$$N_{11}^s \equiv k \int_0^\infty \left[\hat{v}\left(|k-k'|\right) + \hat{v}(k+k')\right] \frac{D\hat{\eta}(k')}{k'}\, dk'. \tag{24}$$

The second remaining term in (21), denoted N_{12}, becomes

$$N_{12}^s \equiv 2k \int_0^k \frac{D\hat{v}(k-k')}{k-k'} \hat{\eta}(k')\, dk'$$

$$- k \int_0^\infty \left\{ \frac{D\hat{v}(|k-k'|)}{|k-k'|} + \frac{D\hat{v}(k+k')}{k+k'} \right\} \hat{\eta}(k')\, dk'. \tag{25}$$

(b) $v_0(-z) = -v_0(z)$.

This corresponds to $\hat{v}(-k') = -\hat{v}(k')$ and $\hat{\eta}(-k') = \hat{\eta}(k')$ and the three terms of (23) add up to

$$N_{11}^a \equiv 2k \int_0^k \hat{v}(k-k')\frac{D\hat{\eta}(k')}{k'}\,dk' - k\int_0^\infty \left[\hat{v}\left(|k-k'|\right)+\hat{v}(k+k')\right]\frac{D\hat{\eta}(k')}{k'}\,dk' \tag{26}$$

and

$$N_{12}^a \equiv k\int_0^\infty \left\{\frac{D\hat{v}(|k-k'|)}{|k-k'|}+\frac{D\hat{v}(k+k')}{k+k'}\right\}\hat{\eta}(k')\,dk'. \tag{27}$$

It is of some interest to note the similarities between the expressions (24)–(27).

To evaluate the integrals in N_{11} and N_{12}, $\hat{v}$ and $\hat{\eta}$ need to be specified. If $\hat{v}$ is split into a symmetric (s) and an anti-symmetric (a) function of y, so that $\hat{v}=\hat{v}_s+\hat{v}_a$, the induced $\hat{\eta}$ becomes $\hat{\eta}_a+\hat{\eta}_s$. The products in (24)–(27) will then contain both symmetric and anti-symmetric parts but by considering values at the centreline of the channel ($y=0$), N_{11} will contain the combination $(\hat{v}_s,\hat{\eta}_a)$ whereas N_{12} contains $(\hat{v}_a,\hat{\eta}_s)$. In the example below, we show results only for the $(\hat{v}_s,\hat{\eta}_a)$-case as this corresponds to the largest transient growth. Thus, only N_{11}^s and N_{11}^a are considered.

$\hat{v}$ is related to the eigenfunctions (ϕ) of the Orr–Sommerfeld equation by $\hat{v}=\sum\phi_n e^{-i\alpha c_n t}$, but only the least damped eigenfunction is chosen in this study. The symmetric eigenfunction is; cf. [5]

$$\phi_s = S\left(\cos\bar{\gamma}\,y-\frac{\cos\bar{\gamma}}{\cosh k}\cosh ky\right) \tag{28}$$

where $\bar{\gamma}$ is solved (with an iterative technique) from the eigenvalue relation

$$\bar{\gamma}\tan\bar{\gamma} = -k\tanh k \tag{29}$$

and

$$S^2 = \frac{2k^2}{(\bar{\gamma}^2+k^2)(1+\sin 2\bar{\gamma}/2\bar{\gamma})}. \tag{30}$$

S is a normalization constant chosen originally such that the initial kinetic energy density of the eigenfunction is unity i.e.

$$\int_0^1 \left\{|\phi|^2+\frac{1}{k^2}|D\phi|^2\right\}dy = 1. \tag{31}$$

The corresponding induced $\hat{\eta}$ becomes

$$\hat{\eta}_a = -ikR\left(\bar{\gamma}^2+k^2\right)S \times\sum_n\left(e^{-\bar{\sigma}t/R}-e^{-\sigma_n t/R}\right)\sin(\gamma_n y)\frac{4\gamma_n\cos\gamma_n}{(\gamma_n^2+k^2)(\bar{\gamma}^2-\gamma_n^2)^2} \times\left[\cos\bar{\gamma}-2\bar{\gamma}\sin\bar{\gamma}\left(\frac{1}{\bar{\gamma}^2-\gamma_n^2}-\frac{1}{\gamma_n^2+k^2}\right)\right] \tag{32}$$

where $\gamma_n=n\pi$ $(n=1,2,\ldots)$, $\sigma_n=\gamma_n^2+k^2$ and $\bar{\sigma}=\bar{\gamma}^2+k^2$.

The normalization (31), however, gives a finite value of ϕ as $k\to\infty$ ($S\approx\sqrt{2}(1+1/2k+\cdots)$) and does not produce converging convolution integrals. Therefore, the normalization in (31) was modified to include a high wave-number cut-off so as to ensure convergence. The function chosen was

$$F = \frac{1}{k_0}\sqrt{\frac{2}{\pi}}\,e^{-k^2/2k_0^2} \tag{33}$$

where k_0 is the position of the inflexion point and the integral over k is unity. (30) was thus modified to

$$S^2 = \frac{2k^2}{(\bar{\gamma}^2+k^2)(1+\sin 2\bar{\gamma}/2\bar{\gamma})}F. \tag{30′}$$

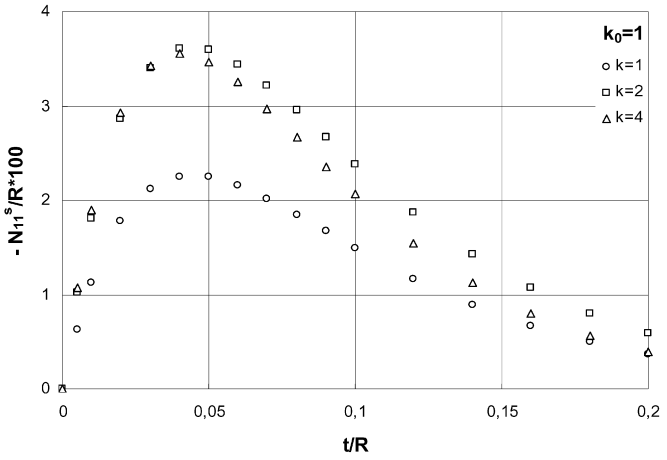

(a)

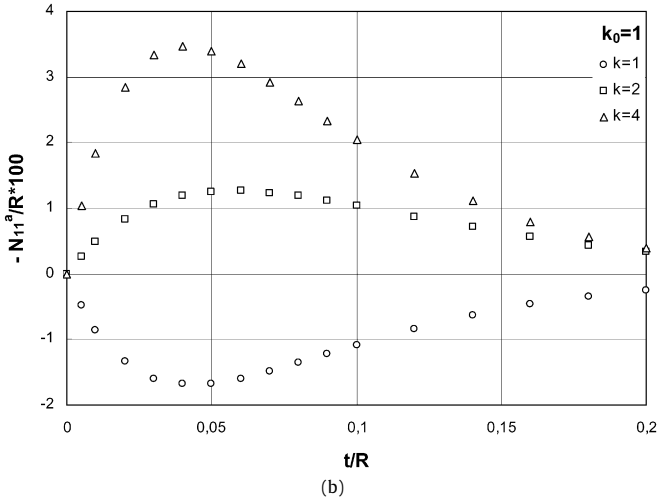

(b)

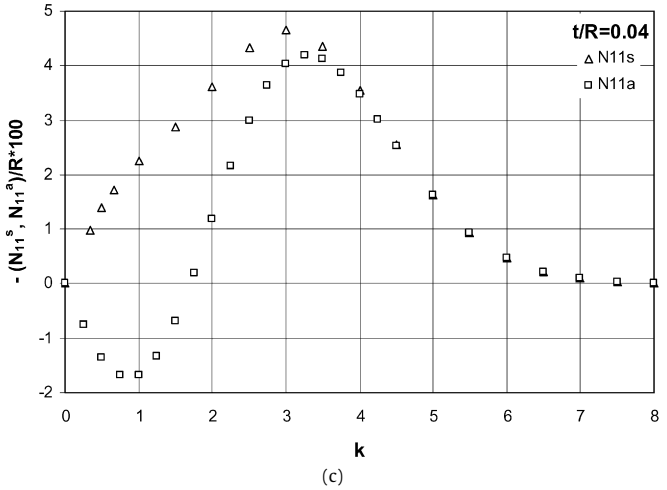

(c)

Fig. 5. Non-linear response in N_{11} as a function of k and t/R. (a) N_{11}^s vs. t/R; $k_0=1$, $k=1,2,4$; (b) N_{11}^a vs. t/R; $k_0=1$, $k=1,2,4$; (c) N_{11}^s and N_{11}^a vs. k for $t/R=0.04$; $k_0=1$.

To evaluate the integrals, the integrands were first tabulated at typically 480 points, up to $k'=20$. Six vorticity modes were used in the summation which was found to represent the full numerical solution to at least 4 significant digits. A standard numerical quadrature technique was then used to evaluate the integrals.

First, the temporal development of N_{11}^s and N_{11}^a was calculated for $k=1$, 2 and 4, with $k_0=1$. These k-values were chosen from Fig. 3b in [5] and represent values to the left, close to

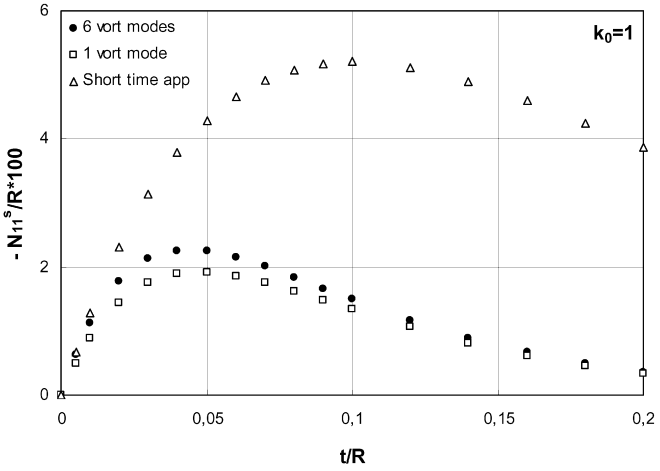

Fig. 6. Comparison between exact numerical solution of N_{11}^s and two approximations: 1 vorticity mode and (linear) short time expansion.

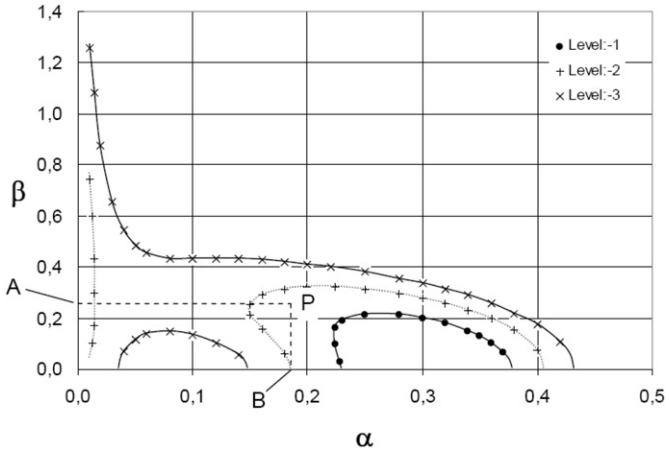

Fig. 7. Level curves of αRc_i for the least damped Orr–Sommerfeld mode in a Blasius boundary layer at $R_{\delta^*} = 500$. Decay rate lower at P than at B.

the top, and to the right of the peak of the energy density of the transiently induced normal vorticity. The results are shown in Figs. 5(a) and 5(b). From the figures, it is noteworthy that the non-linear terms peak at a much smaller time than the linear solution ($t/R \approx 0.084$), and that N_{11}^a may attain both positive and negative values. The shorter time scale may be understood from the fact that the convolution integrands consist of a product of a damped O–S mode and vorticity which peaks and then decays. The product must then get a maximum at a shorter time.

In Fig. 5(a), the peak amplitudes occur for $t/R \approx 0.04$ and for this t/R-value N_{11}^s and N_{11}^a are plotted vs. k in Fig. 5(c). For N_{11}^s the maximum is seen to occur for $k \approx 3$, where the higher value is to be expected from the general tendency of non-linear effects to appear at a shorter length scale ($k_0 = 1$). The behaviour of N_{11}^a is more complicated since it attains both positive and negative values. Thus, there is a certain k-value with no non-linear effect. The precise value varies only slightly with t/R and is in the interval $k = 1.74$–1.62 for $t/R = 0.01$–0.1.

The character of the above results does not change with k_0 but the maximum amplitudes and the k-values at the peaks increase with k_0. E.g. the peak in Fig. 5(c) for N_{11}^s is shifted to $k \approx 5.5$ at $k_0 = 3$.

The fact that the maximum non-linear response occurs at a shorter time than the maximum in the linear problem, suggests that the short time behaviour of (32), i.e. $\hat{\eta} = -\mathrm{i}\beta U' \hat{v}_0 t$ ([14], p. 105) could be used to capture the initial phase of N_{11}^s. The result is shown in Fig. 6. At the peak value in Fig. 5(b), the linear approximation is seen to overestimate the exact value well over 50% and reaches its maximum at a much later time. The temporal behaviour can be understood from the observation that when using the short-time approximation for $\hat{\eta}$, the only damping in the convolution integrand comes from $\hat{v}$ so the product gets a time-scale given by $\hat{v}$. In the figure, the result using just *one* vorticity mode in the sum (32) is also shown. This approximation has a similar temporal behaviour as the exact solution and a slightly lower amplitude.

5. Discussion

In the numerical example shown, the non-linear effects appear at a much shorter time-scale than that for the linear development of the induced vorticity. This result should be expected also for the other non-linear term involving $\hat{\eta}$ and $\hat{v}$, i.e. (18). Since this term should be the dominant for regeneration of $\hat{v}$, the decay properties of the participating $\hat{v}$, and its relation to the transient growth of $\hat{\eta}$, is of particular interest.

Given that the exponential growth rate of TS waves is rather weak for non-inflexional velocity profiles above the critical Reynolds number, it may correspondingly be expected that the *decay rate* at subcritical Reynolds numbers is also small. This was investigated for the least damped Orr–Sommerfeld mode in Blasius flow and the results are shown in Fig. 7. The figure shows level curves in the (α, β) plane of αRc_i at $R = 500$ (based on the displacement thickness, δ^*). αRc_i is a normalized growth rate the use of which is motivated by the temporal amplitude evolution which is $e^{\alpha c_i t}$. Using the temporal scaling of transient growth, t/R, this may also be written as $e^{\alpha Rc_i t/R}$. From [1] it is known that the global optimal occurs for $\tau = 778$ at $R_{\delta^*} = 1000$ ($\alpha = 0$, $\beta = 0.65$). Then, $t/R = 0.778$ and values of αRc_i of -1, -2, -3 give at that time amplitudes 46%, 21% and 9.7%, respectively, of the initial amplitude. Thus, by the time the optimal is reached only wave numbers with the smallest αRc_i values survive and can interact with the normal vorticity at $\alpha = 0$. However, it was also noted in [1] that there is a substantial transient growth for times much smaller than the optimal. E.g. the best optimal at $t/R = 0.1$ ($\alpha = 0.15$, $\beta = 0.96$) has an energy amplification of 43% of the global. For this time, $\alpha Rc_i = -1$, -2, -3 give 91%, 82% and 74%, respectively, of the initial amplitude. Thus, a non-linear interaction between $\hat{v}$ and transiently growing $\hat{\eta}$ may occur given the initial amplitudes are sufficient. A particular feature of this interaction is due to the kidney-shape of the damping curves, as shown in Fig. 7. With $\mathbf{k}'$ at A (on the β-axis) and $\mathbf{k}''$ at B (on the α-axis) the resulting interaction occurs at P where the decay rate is *lower* than at B.

The suggested interaction between $\hat{\eta}$ and $\hat{v}$ may in fact help to explain the relative success of the oblique transition model of Schmid and Henningson [15], where two oblique waves, $(1, 1)$ and $(1, -1)$, are first made to non-linearly produce a $(0, 2)$ component which is then subject to (linear) transient growth. The non-linear interaction would be possible if the initial $(1, \pm 1)$ components of the normal velocity have sufficient amplitude left to interact with the developing longitudinal structure $(0, 2)$. For this mechanism to be useful in a general transition model, however, it seems necessary to invoke also the wave-propagation properties of the interacting wave-numbers since transition must involve space–time synchronization for energy to be transferred between the wave-numbers. With wave-numbers travelling with the group velocity, details of the dispersion properties of the interacting wave numbers will thus need further studies.

Acknowledgements

This work has in part been sponsored by the Swedish Energy Agency program for energy related fluid mechanics. The author is

indebted to Prof. Hans Åkerstedt and Dr. Niklas Davidsson for helpful discussions on the topic of the work.

Appendix A. Expressions for the non-linear terms in terms of $\hat{v}$ and $\hat{\eta}$

For the different terms in $\hat{N}_v$, according to (13), substitution for $\hat{v}$ and $\hat{\eta}$ gives

$$\begin{aligned}\mathrm{i}\alpha\widehat{uv}+\mathrm{i}\beta\widehat{vw} &= \frac{1}{2\pi}\int_{-\infty}^{\infty}\int_{-\infty}^{\infty}\left\{\mathrm{i}\alpha\left(\frac{\mathrm{i}\alpha'}{k'^2}D\hat{v}'-\frac{\mathrm{i}\beta'}{k'^2}\hat{\eta}'\right)\right.\\ &\quad\left.+\mathrm{i}\beta\left(\frac{\mathrm{i}\beta'}{k'^2}D\hat{v}'+\frac{\mathrm{i}\alpha'}{k'^2}\hat{\eta}'\right)\right\}\hat{v}''\,d\alpha'\,d\beta'\\ &= \frac{1}{2\pi}\iint(-A_1D\hat{v}'+B_1\hat{\eta}')\cdot\hat{v}''\,d\alpha'\,d\beta', \qquad (A.1)\end{aligned}$$

$$\begin{aligned}&\alpha^2\hat{u}^2+\beta^2\hat{w}^2+2\alpha\beta\widehat{uw}\\ &=\alpha^2\hat{u}^2+\alpha\beta\widehat{uw}+\beta^2\hat{w}^2+\alpha\beta\widehat{uw}\\ &=\frac{1}{2\pi}\iint\mathrm{i}(A_1D\hat{v}'-B_1\hat{\eta}')\cdot(\alpha\hat{u}''+\beta\hat{w}'')\,d\alpha'\,d\beta'\\ &=-\frac{1}{2\pi}\iint(A_1D\hat{v}'-B_1\hat{\eta}')\cdot(CD\hat{v}''+B_2\hat{\eta}'')\,d\alpha'\,d\beta'. \qquad (A.2)\end{aligned}$$

Thus, the expression for $\hat{N}_v$ becomes

$$\begin{aligned}\hat{N}_v &= -\frac{1}{2\pi}\left(D^2+k^2\right)\iint(-A_1D\hat{v}'+B_1\hat{\eta}')\cdot\hat{v}''\,d\alpha'\,d\beta'\\ &\quad-\frac{1}{2\pi}D\iint(A_1D\hat{v}'-B_1\hat{\eta}')\cdot(CD\hat{v}''+B_2\hat{\eta}'')\,d\alpha'\,d\beta'\\ &\quad-\frac{1}{2\pi}k^2D\iint\hat{v}'\cdot\hat{v}''\,d\alpha'\,d\beta'. \qquad (A.3)\end{aligned}$$

Sorting the terms in the integrands so that terms with $\hat{v}$ (and derivatives) multiplying $\hat{v}$, $\hat{v}$ multiplying $\hat{\eta}$ and $\hat{\eta}$ multiplying $\hat{\eta}$, denoting them $\hat{v}$–$\hat{v}$, $\hat{v}$–$\hat{\eta}$ and $\hat{\eta}$–$\hat{\eta}$ terms, respectively, gives the following terms (omitting the $1/2\pi$ factor and the integral signs):

$$\hat{v}\text{–}\hat{v}\text{:}\ A_1\left(D^2+k^2\right)(D\hat{v}'\cdot\hat{v}'')-A_1CD(D\hat{v}'\cdot D\hat{v}'')-k^2D(\hat{v}'\cdot\hat{v}''); \qquad (A.4)$$

$$\begin{aligned}\hat{v}\text{–}\hat{\eta}\text{:}\ &-B_1\left(D^2+k^2\right)(\hat{v}''\cdot\hat{\eta}')-A_1B_2D(D\hat{v}'\cdot\hat{\eta}'')\\ &+B_1CD(D\hat{v}''\cdot\hat{\eta}'); \qquad (A.5)\end{aligned}$$

$$\hat{\eta}\text{–}\hat{\eta}\text{:}\ B_1B_2D(\hat{\eta}'\cdot\hat{\eta}''). \qquad (A.6)$$

Similarly, for $\hat{N}_\eta$ according to (14) we obtain

$$\begin{aligned}\hat{N}_\eta &= -\frac{1}{2\pi}\beta\iint(B_1D\hat{v}'+A_1\hat{\eta}')\cdot\left(\frac{\beta''}{k''^2}D\hat{v}''+\frac{\alpha''}{k''^2}\hat{\eta}''\right)d\alpha'\,d\beta'\\ &\quad-\frac{1}{2\pi}\alpha\iint(B_1D\hat{v}'+A_1\hat{\eta}')\cdot\left(\frac{\alpha''}{k''^2}D\hat{v}''-\frac{\beta''}{k''^2}\hat{\eta}''\right)d\alpha'\,d\beta'\\ &\quad+\frac{1}{2\pi}D\iint(B_1D\hat{v}'+A_1\hat{\eta}')\cdot v''\,d\alpha'\,d\beta'. \qquad (A.7)\end{aligned}$$

Sorting, as above, we obtain

$$\hat{v}\text{–}\hat{v}\text{:}\ -B_1CD\hat{v}'\cdot D\hat{v}''+B_1D(D\hat{v}'\cdot\hat{v}''), \qquad (A.8)$$

$$\hat{v}\text{–}\hat{\eta}\text{:}\ -B_1B_2D\hat{v}'\cdot\hat{\eta}''-A_1CD\hat{v}''\cdot\hat{\eta}'+A_1D(\hat{v}''\cdot\hat{\eta}'), \qquad (A.9)$$

$$\hat{\eta}\text{–}\hat{\eta}\text{:}\ -A_1B_2\hat{\eta}'\cdot\hat{\eta}''. \qquad (A.10)$$

In these expressions are introduced the weight factors

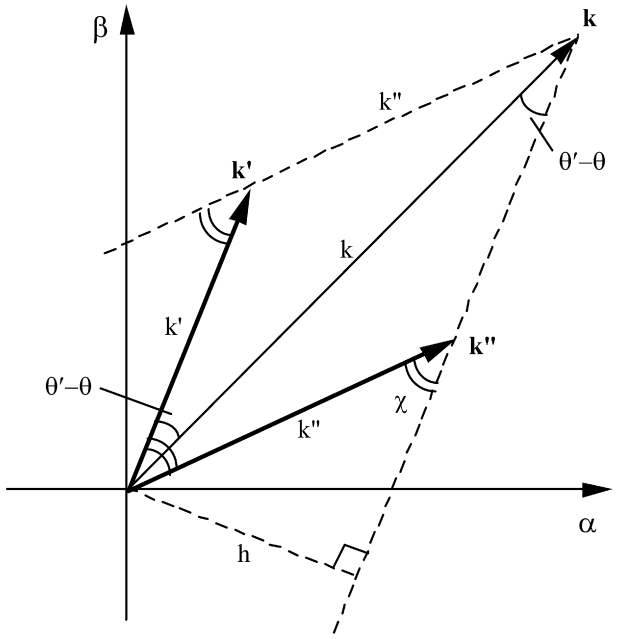

Fig. A1. Geometry for determining interaction factors in convolution integrals.

$$A_1=\frac{\alpha\alpha'+\beta\beta'}{k'^2}, \qquad (A.11a)$$

$$B_1=\frac{\alpha\beta'-\alpha'\beta}{k'^2} \qquad (A.11b)$$

$$A_2=\frac{\alpha\alpha'+\beta\beta'}{k''^2} \qquad (A.11c)$$

$$B_2=\frac{\alpha\beta'-\alpha'\beta}{k''^2} \qquad (A.11d)$$

and

$$C=\frac{k^2}{k''^2}-A_2. \qquad (A.11e)$$

In addition,

$$k''^2=(\alpha-\alpha')^2+(\beta-\beta')^2. \qquad (A.12)$$

These formulas resemble those for periodic perturbations (discrete wave numbers) as presented by Chapman [19].

A.1. Geometric interpretation of the weight factors

Here it is shown how the coefficients in (A.4)–(A.6) and (A.8)–(A.10) can be given simple geometric expressions which helps to evaluate their role in the convolution integration procedure. The strategy is to express them only in k', k'' and χ, the angle between the vectors $\mathbf{k}'$ and $\mathbf{k}''$. First we consider the elementary factors (A.11a)–(A.11d) and use Fig. A1 for definitions.

The following relations hold for the wave numbers:

$$\begin{cases}\alpha=k\cdot\cos\theta,\\ \beta=k\cdot\sin\theta,\end{cases}\qquad\begin{cases}\alpha'=k'\cdot\cos\theta',\\ \beta'=k'\cdot\sin\theta'\end{cases} \qquad (A.13a)$$

$$\Rightarrow\begin{cases}\alpha\alpha'+\beta\beta'=kk'\cdot\cos(\theta'-\theta),\\ \alpha\beta'-\alpha'\beta=kk'\cdot\sin(\theta'-\theta).\end{cases} \qquad (A.13b)$$

Fig. A1 gives

$$\begin{aligned}&k''\cos\chi+k'=k\cos(\theta'-\theta)\\ &\Rightarrow kk'\cos(\theta'-\theta)=k'k''\cos\chi+k'^2. \qquad (A.14)\end{aligned}$$

The cosine theorem:

$$k^2=k'^2+k''^2+2k'k''\cos\chi \qquad (A.15)$$

where χ is the angle between $\mathbf{k}''$ and $\mathbf{k}'$, counted positive from $\mathbf{k}''$ to $\mathbf{k}'$.

For some of the terms (e.g. B_1) it is helpful to use the height h as an intermediary in the analysis since $h/k'' = \sin\chi$. Using these expressions the following results are obtained:

$$A_1 = \frac{\alpha\alpha' + \beta\beta'}{k'^2} = \frac{kk'\cos(\theta' - \theta)}{k'^2} = 1 + \frac{k''}{k'}\cos\chi, \tag{A.16}$$

$$A_2 = \frac{\alpha\alpha' + \beta\beta'}{k''^2} = \frac{kk'\cos(\theta' - \theta)}{k''^2} = \frac{k'^2}{k''^2}\left(1 + \frac{k''}{k'}\cos\chi\right), \tag{A.17}$$

$$B_1 = \frac{\alpha\beta' - \alpha'\beta}{k'^2} = \frac{kk'\sin(\theta' - \theta)}{k'^2} = \frac{h}{k'} = \frac{h}{k''}\frac{k''}{k'} = \frac{k''}{k'}\sin\chi, \tag{A.18}$$

$$B_2 = \frac{\alpha\beta' - \alpha'\beta}{k''^2} = \frac{kk'\sin(\theta' - \theta)}{k''^2} = \frac{hk'}{k''^2} = \frac{k'}{k''}\sin\chi, \tag{A.19}$$

$$C = \frac{k^2}{k''^2} - A_2 = \cdots = 1 + \frac{k'}{k''}\cos\chi, \tag{A.20}$$

$$A_1 C = \cdots = \left(1 + \frac{k''}{k'}\cos\chi\right)\left(1 + \frac{k'}{k''}\cos\chi\right), \tag{A.21}$$

$$A_1 B_2 = \cdots = \sin\chi\left(\frac{k'}{k''} + \cos\chi\right), \tag{A.22}$$

$$B_1 C = \cdots = \sin\chi\left(\frac{k''}{k'} + \cos\chi\right), \tag{A.23}$$

$$B_1 B_2 = \cdots = \sin^2\chi. \tag{A.24}$$

Appendix B. The case of $\alpha = \beta = 0$

The treatment of this case is based on the fact that the Fourier transform, defined as $\hat{f}(\alpha,\beta) = \frac{1}{2\pi}\int_{-\infty}^{\infty}\int_{-\infty}^{\infty} e^{-\mathrm{i}(\alpha x+\beta z)} f(x,z)\,dx\,dz$, becomes $\hat{f}(0,0) = \frac{1}{2\pi}\int_{-\infty}^{\infty}\int_{-\infty}^{\infty} f(x,z)\,dx\,dz \equiv \bar{f}$, where the overbar notation is introduced for simplicity. Thus, the $(0,0)$ component in the Fourier plane corresponds to the integration of the physical quantity in the x–z plane. If this is applied to continuity and the governing equations, assuming that the perturbation is limited in extent with amplitudes decaying sufficiently fast at infinity for the x–z integrals to exist, (6) first produces

$$D\bar{v} = 0. \tag{B.1}$$

Applying the boundary condition on a solid wall then gives $\bar{v} = 0$ throughout the flow and Eq. (8) collapses. Even if Eq. (9) still can be solved, the alternative is to return to the component equations for the physical quantities and integrate in the x–z plane. Then, all x and z derivatives vanish and left are the following equations:

$$\bar{u}_t + D(\overline{uv}) = \frac{1}{R}D^2\bar{u}, \tag{B.2a}$$

$$D(\overline{vv}) = -D\bar{p}, \tag{B.2b}$$

$$\bar{w}_t + D(\overline{wv}) = \frac{1}{R}D^2\bar{w}. \tag{B.2c}$$

Using the definitions for the inverse Fourier transform and the fact that $\int_{-\infty}^{\infty} e^{\mathrm{i}\alpha x}\,dx = 2\pi\,\delta(\alpha)$ then gives

$$\overline{uv} = \frac{1}{2\pi}\iint \hat{u}(\alpha,\beta)\cdot\hat{v}^*(\alpha,\beta)\,d\alpha\,d\beta \tag{B.3}$$

where (C.1b) has been used. Similarly, for $\overline{vw}$ one obtains

$$\overline{vw} = \frac{1}{2\pi}\iint \hat{w}(\alpha,\beta)\cdot\hat{v}^*(\alpha,\beta)\,d\alpha\,d\beta. \tag{B.4}$$

The resulting equations (B.2a) and (B.2c) then obtain the integral form of Eqs. (5.39) and (5.40) in Schmid and Henningson [14], except for the complex conjugate. For the initial, linear development of a perturbation, (B.3) and (B.4) can be rewritten, first using (11) and (12) to substitute $\hat{u}$ and $\hat{w}$ and then the symmetry properties (C.1) and (C.2) to reduce the (α,β) integration to the first quadrant. Then,

$$\overline{uv} = \frac{1}{\pi}\int_0^{\infty}\int_0^{\infty}\left\{\frac{\mathrm{i}\alpha}{k^2}(D\hat{v}\cdot\hat{v}^* - D\hat{v}^*\cdot\hat{v}) + \frac{\mathrm{i}\beta}{k^2}(\hat{v}\cdot\hat{\eta}^* - \hat{v}^*\cdot\hat{\eta})\right\}d\alpha\,d\beta \tag{B.5}$$

and

$$\overline{vw} = 0. \tag{B.6}$$

These expressions apply as long as $\hat{v}$ and $\hat{\eta}$ follow a linear development. The $\mathrm{i}\beta$-term in (B.5) assures that the growth of $\hat{\eta}$ along the β-axis is effectively integrated to a $\overline{uv}$ contribution. This term may be expressed analytically on the β-axis. Finally, the result (B.6) together with (B.2c), shows that $\bar{w}$ simply diffuses from its initial value and will need non-linear interactions to grow.

Appendix C. Symmetry properties of $\hat{v}$ and $\hat{\eta}$ in the (α,β) plane

When performing actual calculations of the convolution integrals in the early (linear) stage of the perturbation development, it may be helpful to use the symmetry properties in the (α,β) plane for linearly evolving $\hat{v}$ and $\hat{\eta}$, to reduce the integrations to the first quadrant. These relations are derived from (8), (9) and the definition of the Fourier transform. From the definition, $\hat{v}(\alpha,\beta) = \frac{1}{2\pi}\int_{-\infty}^{\infty}\int_{-\infty}^{\infty} e^{-\mathrm{i}(\alpha x+\beta z)} v(x,z)\,dx\,dz$, follows that $\hat{v}(-\alpha,-\beta) = \hat{v}^*(\alpha,\beta)$ and $\hat{\eta}(-\alpha,-\beta) = \hat{\eta}^*(\alpha,\beta)$, where * denotes complex conjugate. The complex conjugate of (8) shows that $\hat{v}^*(-\alpha,\beta)$ satisfies the same equation as $\pm\hat{v}(\alpha,\beta)$ and, provided the initial data are the same, equality holds. Again, using the definition of the Fourier transform, it follows that the plus-sign applies if the initial v satisfies $v_0(x,-z) = v_0(x,z)$ and the minus-sign if $v_0(x,-z) = -v_0(x,z)$. With $\hat{v}(\alpha,-\beta) = \hat{v}^*(-\alpha,\beta)$ it thus follows that

$$\hat{v}(-\alpha,\beta) = \pm\hat{v}^*(\alpha,\beta), \tag{C.1a}$$

$$\hat{v}(-\alpha,-\beta) = \hat{v}^*(\alpha,\beta), \tag{C.1b}$$

$$\hat{v}(\alpha,-\beta) = \pm\hat{v}(\alpha,\beta). \tag{C.1c}$$

For $\hat{\eta}$ the corresponding relations are obtained by noting that $-\hat{\eta}(\alpha,-\beta)$ satisfies the same equation as $\hat{\eta}(\alpha,\beta)$ if the plus sign is used in (C.1c) (only $\hat{v}$-induced $\hat{\eta}$ is considered).

Thus,

$$\hat{\eta}(-\alpha,\beta) = \mp\hat{\eta}^*(\alpha,\beta), \tag{C.2a}$$

$$\hat{\eta}(-\alpha,-\beta) = \hat{\eta}^*(\alpha,\beta), \tag{C.2b}$$

$$\hat{\eta}(\alpha,-\beta) = \mp\hat{\eta}(\alpha,\beta). \tag{C.2c}$$

References

[1] K.M. Butler, B.F. Farrell, Three-dimensional optimal perturbations in viscous shear flow, Phys. Fluids A 4 (1992) 1636.
[2] P. Corbett, A. Bottaro, Optimal perturbations for boundary layers subject to stream-wise pressure gradient, Phys. Fluids 12 (2000) 120–130.
[3] J. Kim, J. Lim, A linear process in wall-bounded turbulent shear flows, Phys. Fluids 12 (8) (2000) 1885–1888.
[4] C.F. Pearson, F.H. Abernathy, Evolution of the flow field associated with a streamwise diffusing vortex, J. Fluid Mech. 146 (1984) 271–283.
[5] L.H. Gustavsson, Energy growth of three-dimensional disturbances in plane Poiseuille flow, J. Fluid Mech. 224 (1991) 241–260.
[6] M. Matsubara, P.H. Alfredsson, Disturbance growth in boundary layers subjected to free-stream turbulence, J. Fluid Mech. 430 (2001) 149–168.
[7] A.H. Nayfeh, Effect of stream vortices on Tollmien–Schlichting waves, J. Fluid Mech. 107 (1981) 441–453.

[8] F. Waleffe, Hydrodynamic stability and turbulence: Beyond transients to a self-sustaining process, Stud. Appl. Math. 95 (1995) 319–343.
[9] C. Cossu, L. Brandt, Stabilization of Tollmien–Schlichting waves by finite amplitude optimal streaks in the Blasius boundary layer, Phys. Fluids 14 (8) (2002) L57.
[10] P. Andersson, L. Brandt, A. Bottaro, D.S. Henningson, On the breakdown of boundary layer streaks, J. Fluid Mech. 428 (2003) 29–60.
[11] S.C. Reddy, P.J. Schmid, J.S. Baggett, D.S. Henningson, On stability of streamwise streaks and transition thresholds in plane channel flows, J. Fluid Mech. 365 (1998) 269–303.
[12] C. Cossu, L. Brandt, On Tollmien–Schlichting-like waves in streaky boundary layers, Eur. J. Mech. B/Fluids 23 (2004) 815–833.
[13] J.H.M. Fransson, A. Talamelli, L. Brandt, C. Cossu, Delaying transition to turbulence by a passive mechanism, Phys. Rev. Lett. 96 (2006) 064501.
[14] P.J. Schmid, D.S. Henningson, Stability and Transition in Shear Flows, Springer, 2001.
[15] P.J. Schmid, D.S. Henningson, A new mechanism for rapid transition involving a pair of oblique waves, Phys. Fluids A 4 (1992) 1986–1989.
[16] J.M. Hamilton, J. Kim, F. Waleffe, Regeneration mechanisms of near-wall turbulence structures, J. Fluid Mech. 287 (1995) 317–348.
[17] J. Jimenez, A. Pinelli, The autonomous cycle of near-wall turbulence, J. Fluid Mech. 389 (1999) 335–359.
[18] W. Schoppa, F. Hussain, Coherent structure generation in near-wall turbulence, J. Fluid Mech. 453 (2002) 57–108.
[19] S.J. Chapman, Subcritical transition in channel flows, J. Fluid Mech. 451 (2002) 35–97.
[20] E.N. Davidsson, Stability and transition in the suction boundary layer and other shear flows, Doctoral thesis 2007:04, Luleå University of Technology.